

Full-Field Electroretinography, Pupillometry, and Luminance Thresholds in X-Linked Retinoschisis

J. Jason McAnany,^{1,2} Jason C. Park,¹ Gerald A. Fishman,^{1,3} and Frederick T. Collison³

¹Department of Ophthalmology and Visual Sciences, University of Illinois at Chicago, Chicago, Illinois, United States

²Department of Bioengineering, University of Illinois at Chicago, Chicago, Illinois, United States

³The Pangere Center for Inherited Retinal Diseases, The Chicago Lighthouse, Chicago, Illinois, United States

Correspondence: J. Jason McAnany, Department of Ophthalmology and Visual Sciences, University of Illinois at Chicago, 1855 W. Taylor Street, MC/648, Chicago, IL 60612, USA; jmcana1@uic.edu.

Received: April 13, 2020

Accepted: May 21, 2020

Published: June 24, 2020

Citation: McAnany JJ, Park JC, Fishman GA, Collison FT. Full-field electroretinography, pupillometry, and luminance thresholds in X-linked retinoschisis. *Invest Ophthalmol Vis Sci.* 2020;61(6):53. <https://doi.org/10.1167/iovs.61.6.53>

PURPOSE. To evaluate the nature and extent of functional abnormality in X-linked retinoschisis (XLRS) by comparing three dark-adapted, full-field measures: the electroretinogram (ERG), pupillary light reflex (PLR), and luminance threshold.

METHODS. ERGs, PLRs (pupil constriction due to light stimulation), and luminance thresholds were measured from seven XLRS subjects and from 10 normally sighted, age-similar controls. ERGs and PLRs were obtained for a range of flash strengths, and these data were fit with Naka–Rushton functions to derive the maximum saturated b-wave (V_{\max}) and PLR (P_{\max}) amplitudes. Additionally, semi-saturation constants were obtained for the b-wave (σ) and PLR (s). Values of $1/\sigma$ and $1/s$ provide sensitivity measures. Full-field, dark-adapted luminance thresholds were measured using 465-nm and 642-nm flash stimuli.

RESULTS. V_{\max} and $1/\sigma$ were significantly reduced in XLRS compared to the controls (both $t \geq 5.33$, $P < 0.001$). In comparison, P_{\max} was normal in the XLRS subjects ($t = 1.39$, $P = 0.19$), but $1/s$ was reduced ($t = 7.84$, $P < 0.001$). Luminance thresholds for the control and XLRS groups did not differ significantly ($F = 3.57$, $P = 0.08$). Comparisons among measures indicated that pupil sensitivity was correlated with luminance threshold for the long- and short-wavelength stimuli (both, $r \geq 0.77$, $P \leq 0.04$). Correlations among all other measures were not statistically significant.

CONCLUSIONS. The results indicate that the presumed bipolar cell dysfunction in XLRS, indicated by b-wave abnormalities, has complex downstream effects: Dark-adapted luminance threshold and maximum pupil responses are not significantly affected, but pupil sensitivity is reduced.

Keywords: X-linked retinoschisis, electroretinogram, pupillary light reflex, luminance threshold








X-linked retinoschisis (XLRS) is a juvenile-onset vitreo-retinal degenerative disease that is caused by mutations in the *Retinoschisin 1 (RS1)* gene.^{1–3} XLRS is characterized clinically by cystic-appearing macular lesions and visual acuity loss in the first or second decade of life.^{2,4,5} In addition, approximately 50% of patients also develop peripheral retinoschisis, most frequently in the temporal retina.² The full-field electroretinogram (ERG) is often useful in the diagnosis of XLRS because the b-wave amplitude can be reduced disproportionately in comparison to the a-wave amplitude under dark-adapted conditions.^{6,7} This characteristic “electronegative” response pattern suggests a post-receptor defect, which is supported by findings showing protein deficiency and structural abnormality at the photoreceptor–bipolar cell synapse.^{8,9} Although b-wave amplitude loss is commonly reported in these individuals, smaller than normal a-wave amplitudes and reduced rod-saturated photoresponse amplitudes have also been reported.^{6,7,10} Consistent with these clinical findings, rod and cone degeneration has been reported in mouse models of XLRS.⁹ Thus, in addition to the well-documented abnor-

malities in post-receptor function, the response of the photoreceptors can be abnormal in human XLRS patients and in animal models of the disease.

In contrast to the marked ERG and structural abnormalities, luminance thresholds measured across the visual field under dark-adapted conditions have been reported to be normal or only mildly elevated.⁷ Psychophysical thresholds under mesopic conditions appear to be more variable among individuals with XLRS. Specifically, microperimetric sensitivity was reported to be elevated in some XLRS subjects and within the normal range for others.¹¹ An important consideration in comparing previous studies is that the ERG b-wave amplitude loss has been assessed using diffuse full-field stimuli, whereas psychophysical luminance threshold measurements have been performed with spatially discrete targets (e.g., Goldmann target sizes III or V). To date, full-field luminance thresholds have not been measured and compared to full-field ERG responses in XLRS subjects.

Likewise, a third full-field measure of function—pupillary light reflex (PLR), the response of the pupil to a flash of light—has not been reported in XLRS, but this measure may

TABLE. Subject Characteristics

Subject No.	Color Code	Age (y)	Acuity (logMAR)	RS1 Variant
1		23	0.38	Not available
2		34	0.56	c.578C>T (p.Pro193Leu)
3		38	0.30	Not available
4		19	0.68	c.218C>A (p.Ser73*)
5		40	0.40	c.208G>A (p.Gly70Ser)
6		37	0.66	c.208G>A (p.Gly70Ser)
7		21	0.58	c.-35_522+?del

provide insight into functional deficits in these individuals. PLR measurement has parallels to ERG measurement in that it can be recorded under dark- and light-adapted conditions to assess rod and cone pathway function. Responses under these conditions have been reported in several other forms of inherited retinal degenerative disease.^{12–14} In addition to rod- and cone-mediated PLRs, the post-illumination pupil response (PIPR) can be assessed to provide a more direct measure of inner-retina function. The PIPR is thought to be generated by the activation of melanopsin, a photopigment contained within intrinsically photosensitive retinal ganglion cells (ipRGCs).^{15,16} Abnormalities of the PIPR in XLRs would suggest dysfunction of the inner retina.

The purpose of the present study was to record and compare three full-field functional measures in individuals diagnosed with XLRs: ERG, luminance threshold, and PLR. The ERG and PLR measurements were performed across a broad range of stimulus strengths to gain a better understanding of how the extent of abnormality varies for different stimuli. We were particularly interested in evaluating the apparent discrepancy between the dark-adapted ERG, which is typically abnormal, and the dark-adapted psychophysical luminance threshold, which has been reported to be normal in these individuals. Thus, we sought to provide a comprehensive analysis of dark-adapted retinal function assessed using full-field stimuli in XLRs.

METHODS

Subjects

The research followed the tenets of the Declaration of Helsinki and was approved by institutional review boards at the University of Illinois at Chicago and by the Western Institutional Review Board (The Chicago Lighthouse). All subjects provided written informed consent prior to participating. Seven male subjects with a clinical diagnosis of XLRs were recruited from the cohort of The Chicago Lighthouse (ages, 19–40 years). The clinical diagnosis of XLRs was based on typical fundus features, including a spoke-wheel pattern of macular schisis, cystic-appearing macular lesions on OCT, and functional abnormalities including visual acuity loss and a reduced ERG b-/a-wave amplitude ratio. Five of the seven subjects were genotyped, and a mutation in the *RS1* gene was confirmed in each of these five individuals. The Table lists the age, visual acuity, and *RS1* mutation (when available) for the XLRs subjects.

Ten visually normal control subjects (five male and five female; ages, 24–41 years) with no history of eye

disease, with Early Treatment Diabetic Retinopathy Study best-corrected visual acuity of 0 logMAR or better, and with normal contrast sensitivity as assessed by the Pelli–Robson chart also participated in the study. ERG, PLR, and luminance threshold data were obtained from each of the 10 control subjects. An independent samples *t*-test indicated that the mean age of the controls did not differ significantly from that of the XLRs subjects ($t = 0.05$, $P = 0.96$).

Apparatus, Stimuli, and Procedure

All stimuli were generated by and presented in a commercially available ColorDome Desktop Ganzfeld system (Diagnosys LLC, Lowell, MA, USA). The spectral characteristics of the stimuli were measured with a PR-740 SpectraScan spectroradiometer (Photo Research/JADAK, Inc., Syracuse, NY, USA), and luminance values were calculated based on $V_{10\lambda}$. For all three tests, measurements were performed monocularly, with the fellow eye patched. Pupil measurements were performed with natural pupils, whereas the ERG and luminance threshold measurements were performed after pupil dilation with 2.5% phenylephrine hydrochloride and 1% tropicamide drops.

Electroretinogram Measurement

ERGs were recorded using DTL corneal electrodes (Diagnosys, LLC), with gold-cup electrodes used as reference (ear) and ground (forehead). Amplifier bandpass settings were 0.30 to 500 Hz, and the sampling frequency was 2 kHz. Following adaptation to a uniform achromatic field (30 cd/m²), light-adapted responses were elicited by light-emitting diode (LED)-generated achromatic 3.0 cd·s·m⁻² flash (4 ms) and flicker (31.25 Hz) stimuli. Subjects were then dark-adapted for 20 minutes, and responses were elicited by LED-generated achromatic flashes (4 ms) that ranged from 0.0001 to 10.0 cd·s·m⁻². For each stimulus strength, a minimum of three responses were obtained and averaged for analysis.

The ERGs were analyzed by plotting the b-wave amplitude as a function of log stimulus time-integrated luminance (L), and fitting the data with Equation 1 to extract V_{\max} (the maximum saturated b-wave amplitude) and σ (the b-wave semi-saturation constant). The value of $1/\sigma$ provides a measure of b-wave sensitivity.^{17,18}

$$V = V_{\max} [L / (L + \sigma)] \quad (1)$$

Of note, Equation 1 was only fit to the four lowest time-integrated flash luminances, as intrusion of the a-wave

affects the b-wave amplitude at higher flash strengths.¹⁹ The values of V_{\max} and σ were determined by minimizing the mean squared error between the data and the fit.

Pupil Measurements. Each subject underwent full-field pupillometry recording, using methods that have been described elsewhere.¹² In brief, subjects were dark-adapted for 10 minutes, and the response of the pupil to flashes of long-wavelength light (1 second in duration; 642-nm peak wavelength) was recorded using an infrared videography system. Stimulus luminance ranged from 0.0001 to 450 cd/m². At least two responses for each stimulus luminance were obtained and averaged for analysis. To minimize the effects of inter-subject differences in baseline pupil size, the pupil diameter was normalized by the mean baseline pupil size during the 1 second preceding the flash. The transient PLR amplitude was defined as the difference between the normalized baseline diameter and the maximal pupillary constriction following the stimulus onset.

For analysis, the transient PLR amplitude was plotted as a function of log stimulus luminance and the data were fit with the following function to extract P_{\max} (the maximum saturated PLR amplitude) and s (the PLR semi-saturation constant). The value of $1/s$ provides a measure of pupil sensitivity:

$$PLR = P_{\max} \left[L^n / (L^n + s^n) \right] \quad (2)$$

where L is the stimulus luminance and n is the slope of the function. Of note, this is similar to Equation 1, with the exception of the n parameter. The value of n was set to 0.43 (mean value for the control subjects), and P_{\max} and s were determined by minimizing the mean squared error between the data and the fit.

In addition to measuring the transient PLR, the PIPR was recorded for each subject. The PIPR is a sustained pupillary constriction that follows the offset of a high-luminance, short-wavelength flash. This response component is thought to be mediated by activation of the melanopsin photopigment that is contained in ipRGCs.^{15,20–22} A 450-cd/m² short-wavelength (465-nm peak) flash that was 1 second in duration was used to elicit the PIPR. Pupil size was normalized by the baseline pupil diameter, as described above, and PIPR amplitude was defined as the median normalized pupil size from 5 to 7 seconds following the flash (6–8 seconds after the 1-second flash onset) in accordance with previous definitions.^{23,24}

Luminance Threshold Measurement. Following 30 minutes of dark adaptation, thresholds were measured in response to full-field flashes of long-wavelength (642 nm) and short-wavelength (465 nm) light. The full-field stimulus test (FST) protocol (provided by Diagnosys and described in detail elsewhere²⁵) was used to measure thresholds for these stimuli. In brief, 4-ms flashes of light were presented within the ColorDome Desktop Ganzfeld system, and the subject was asked to indicate, by button press, if the stimulus was perceived. The FST software plots percent detection as a function of log time-integrated flash luminance and fits the data with a Weibull function to define threshold. In the figures shown below, 0 dB is equal to 0.01 cd·s·m⁻², and thresholds for the long- and short-wavelength stimuli were based on the mean of two measurements for each wavelength.

RESULTS

ERG Data

Figure 1 shows ERG waveforms for the seven XLRs subjects under the minimum recommended International Society for Clinical Electrophysiology of Vision (ISCEV) standard conditions.²⁶ The gray boxes represent the instrument-specified normal range for the responses, and the black traces are from a representative control. For the dark-adapted 0.01 cd·s·m⁻² stimulus (Fig. 1A), the b-wave amplitude was within the lower limit of normal for two subjects and was subnormal for the other five. The a-wave elicited by the dark-adapted 3.0 cd·s·m⁻² stimulus (Fig. 1B) was within the range of normal for all subjects. In contrast, the b-wave was reduced, with the exception of two subjects who had amplitudes near the lower limit of normal. The light-adapted responses (Figs. 1C, 1D) were also abnormal for the seven subjects. That is, the light-adapted 3.0 cd·s·m⁻² a-wave tended to be at the lower limit of normal; the b-wave was delayed in all seven subjects and was reduced in amplitude for six subjects (Fig. 1C). The flicker responses (Fig. 1D) were attenuated and delayed in all seven XLRs subjects. In general, these responses are typical of XLRs subjects and highlight the previously reported ERG variation among these individuals.^{2,27–29}

Figure 2 shows the ERG b-wave amplitude for each stimulus luminance under dark-adapted conditions for each of the seven XLRs subjects (top panel) and the mean (± 1 SEM) control response (black circles). The solid lines are the fits of Equation 1 to the data, as described above. In general, the XLRs subjects had reduced b-wave amplitudes for each time-integrated flash luminance. The exception was XLRs1, who had responses of normal amplitude for the highest time-integrated flash luminances; however, these apparently normal b-wave amplitudes are primarily due to this subject's large a-wave. For low time-integrated flash luminances, the b-wave amplitudes varied among the subjects, ranging from a moderate loss (XLRs1, XLRs4) to profound loss (XLRs2, XLRs6, XLRs7). This pattern of response resulted in the patients' fits being compressed and shifted rightward relative to the control mean. V_{\max} and σ were derived to quantify this pattern and to estimate the maximum saturated b-wave amplitude and sensitivity. These data are shown in the lower panel, which plots $\log \sigma$ as a function of $\log V_{\max}$. This panel shows that σ was increased (sensitivity was reduced) for the XLRs subjects compared to the controls. In addition, V_{\max} was typically reduced for the XLRs subjects. Only XLRs1 had values of σ and V_{\max} that were within the lower limit of normal. Independent sample t -tests were performed to compare statistically $\log \sigma$ and $\log V_{\max}$ for the control and XLRs groups. The t -tests indicated a significant reduction in $\log V_{\max}$ ($t = 5.73$, $P < 0.001$) and an increase in $\log \sigma$ ($t = 5.33$, $P < 0.001$).

It is also apparent that there is a strong correlation between $\log \sigma$ and $\log V_{\max}$ for the XLRs subjects, such that subjects with the smallest V_{\max} had the lowest sensitivity ($r = -0.94$, $P = 0.002$). The solid line is a linear regression fit to the XLRs subject data. Although the correlations between these parameters is strong, it should be noted that some subjects had marked amplitude reductions (e.g., XLRs2, XLRs6, XLRs7) that limited the number of data points that could be fit, which consequently reduces confidence in the fit parameters. Nevertheless, the data clearly show that the b-wave amplitude can be abnormal in XLRs, as expected,

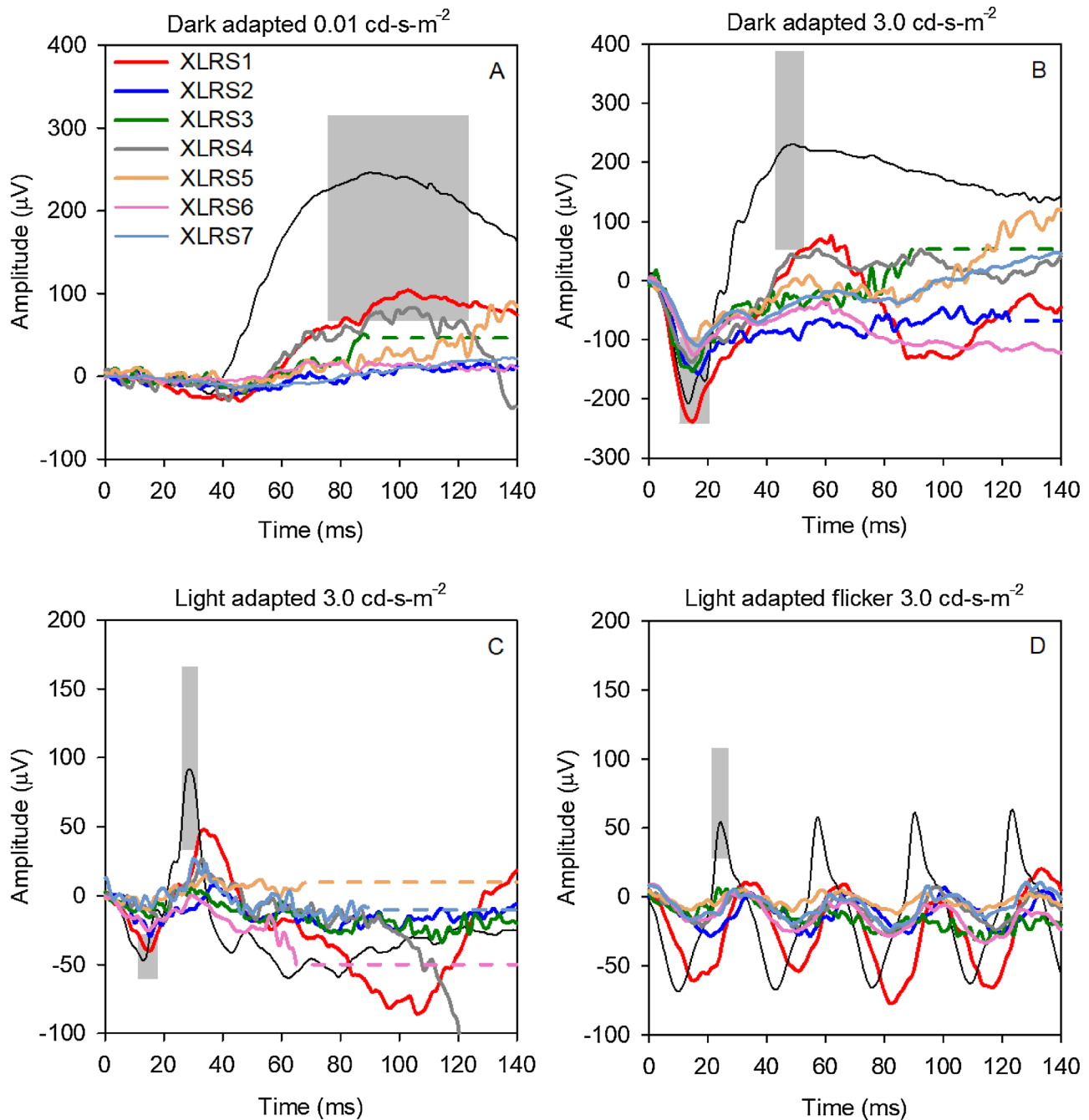


FIGURE 1. ERG waveforms are shown for each XLRS subject (color coding as indicated by the key) and a representative control subject (*black traces*). The four ISCEV standard conditions are shown: dark-adapted 0.01 cd-s-m^{-2} (**A**) and 3.0 cd-s-m^{-2} (**B**), as well as light-adapted single flash (**C**) and flicker (**D**) (both, 3.0 cd-s-m^{-2}). The *gray boxes* mark the normal limits.

and the abnormality is characterized by a reduced maximum amplitude (V_{\max}) and reduced sensitivity ($1/\sigma$).

PLR Data

Figure 3 (top panel) shows the PLR amplitude for each stimulus luminance for each of the seven XLRS subjects and the mean (± 1 SEM) control response (black circles). The solid lines are the fits of Equation 2 to the data, as described above. In general, each of the seven subjects had reduced PLR amplitude for low to moderate stimulus lumi-

nances. The PLR was either normal (XLRS2, XLRS3, XLRS5) or approached the normal mean (XLRS1, XLRS4, XLRS6, XLRS7) for the highest stimulus luminances. This pattern of response resulted in the patients' fits being shifted rightward with minimal compression relative to the control mean. P_{\max} and s were derived to quantify this pattern and estimate the maximum saturated pupil amplitude and sensitivity. These data are shown in the lower panel, which plots $\log s$ as a function of P_{\max} . This panel shows that s was increased (sensitivity reduced) for each XLRS subject (patient data are shifted upward relative to the controls). By contrast, P_{\max}

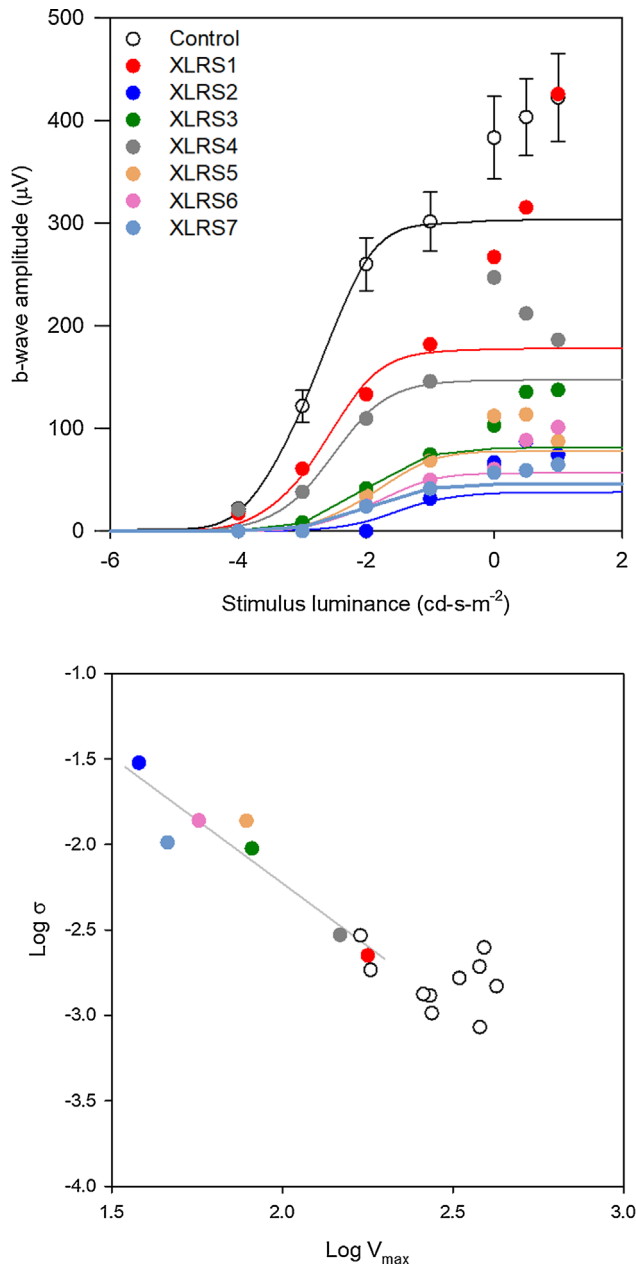


FIGURE 2. ERG b-wave amplitude is plotted as a function of log stimulus time-integrated luminance (*top panel*) for each XLRs subject and the mean (± 1 SEM) control response (color-coding conventions are given in the Table). The *lower panel* shows $\log \sigma$ as a function of $\log V_{\max}$ for each XLRs and control subject. The *solid line* is a linear regression fit to the XLRs data.

was normal in four XLRs subjects and slightly reduced below the lower limit of normal in the other three (less than 1% below the lower limit, on average). Independent sample *t*-tests were performed to compare statistically $\log s$ and P_{\max} for the control and XLRs groups. The *t*-tests indicated a significant increase in $\log s$ ($t = 7.84$, $P < 0.001$) but no significant P_{\max} reduction ($t = 1.39$, $P = 0.19$). Thus, the data show that the pupil response can be abnormal in XLRs, and the abnormality is best characterized by reduced sensitivity ($1/s$). Consistent with the ERG b-wave data discussed above, it is also apparent that there is a strong correlation between

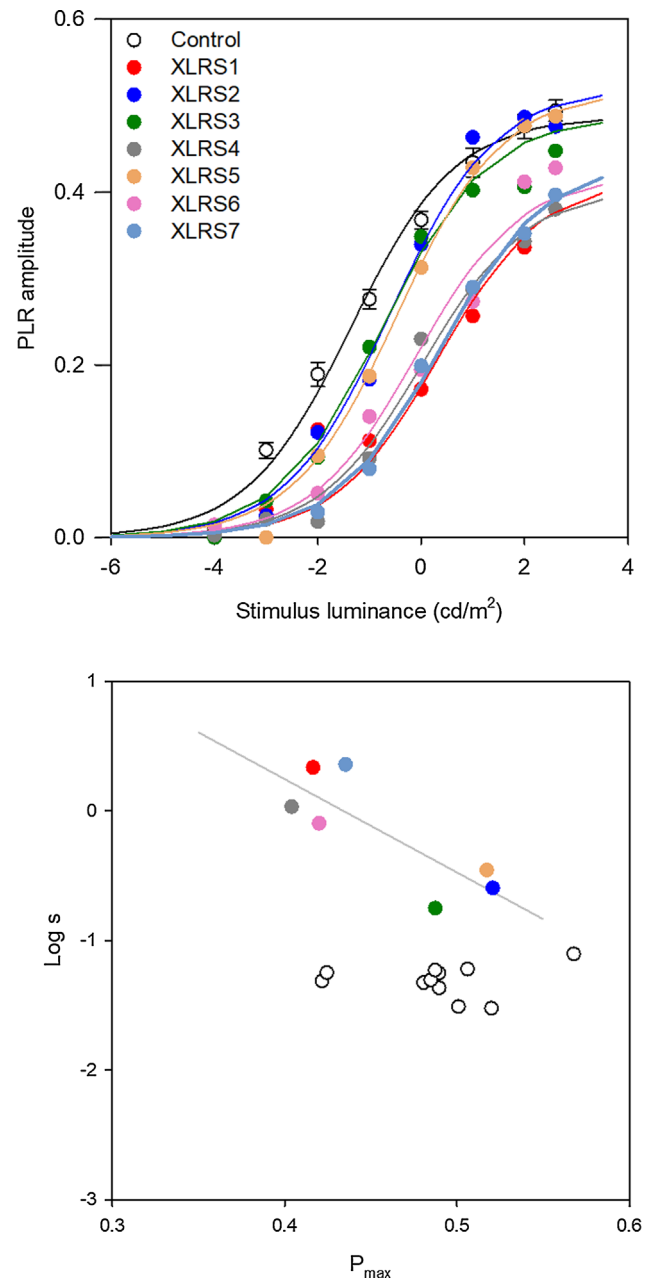


FIGURE 3. PLR amplitude is plotted as a function of log stimulus luminance (*top panel*) for each XLRs subject and the mean (± 1 SEM) control response (color-coding conventions are given in the Table). The *lower panel* shows $\log s$ as a function of P_{\max} for each XLRs and control subject. The *solid line* is a linear regression fit to the XLRs data.

$\log s$ and P_{\max} for the XLRs subjects, such that subjects with the lowest sensitivity also had the smallest P_{\max} ($r = -0.81$, $P = 0.03$).

Figure 4 shows the normalized pupil response elicited by a 450-cd/m² short-wavelength flash (top) and a 450-cd/m² long-wavelength flash (bottom). The range of responses of the 10 control subjects for each wavelength is indicated by the gray area, and the normalized pupil size over time for each XLRs subject is shown by the color-coded traces. For the short-wavelength flash, the initial transient constriction was within the normal range for all subjects

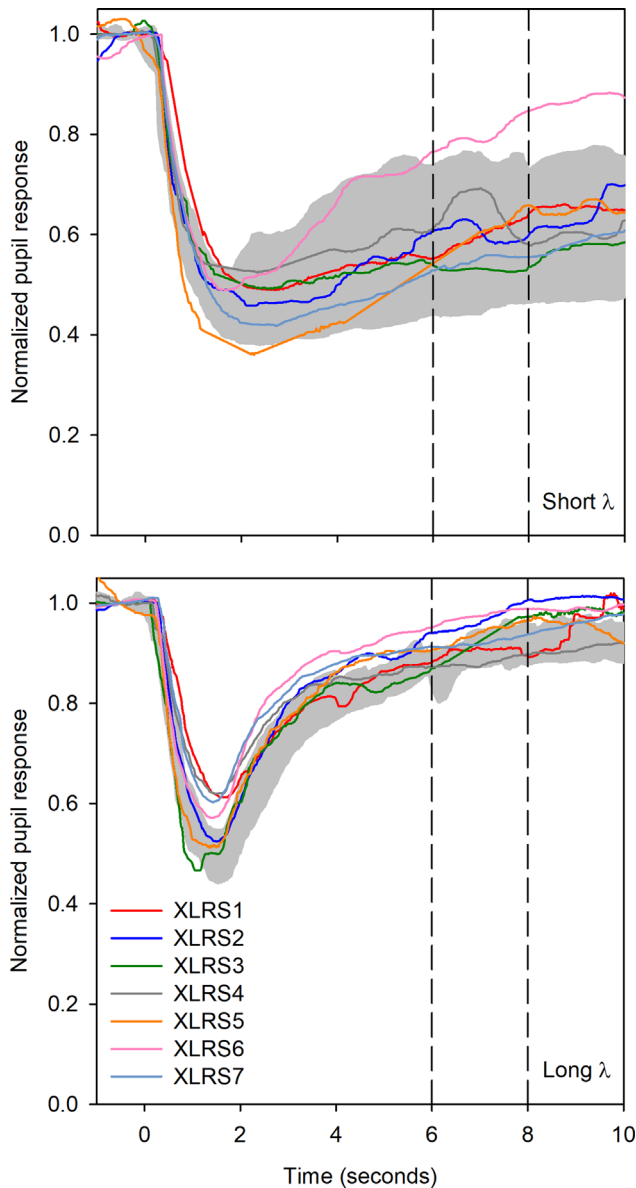


FIGURE 4. Normalized pupil diameter over time following a 1-second 450-cd/m² short-wavelength flash (*top*) and a 1-second 450-cd/m² long-wavelength flash (*bottom*). The gray regions show the control range (minimum to maximum), and the color-coded traces represent the pupil response for each XLRs subject. The PIPR is measured 5 to 7 seconds after the offset of the stimulus (6 to 8 seconds after stimulus onset) as indicated by the vertical dashed lines.

(perhaps slightly super-normal for XLRs5). The PIPR component of the response (dashed lines) was within the range of normal for all subjects except XLRs6. For this subject, the median normalized pupil size was reduced by approximately 7% below the lower limit of normal. For the long-wavelength flash (Fig. 4, bottom), four of the seven subjects had a transient response component within the normal range. The reductions in the three other subjects were small (less than 4% on average; see also Fig. 3, bottom). Note also that the PIPR elicited by the long-wavelength stimulus was generally negligible for both the control and XLRs subjects.

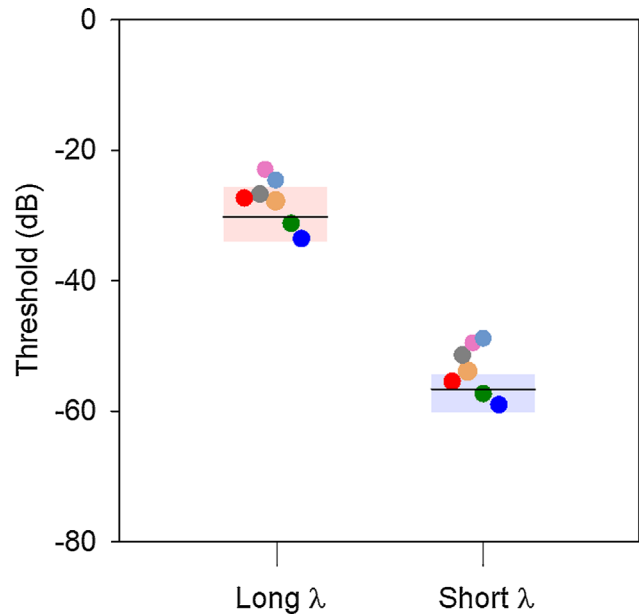


FIGURE 5. FST threshold is shown for each XLRs subject for the long-wavelength stimulus (*left*) and short-wavelength stimulus (*right*) (color-coding conventions are given in the Table). The range of controls for the long- and short-wavelength stimuli are shown by the boxes; the horizontal lines mark the control mean.

FST Data

Figure 5 shows thresholds (dB) measured with the long-wavelength (left) and short-wavelength (right) stimuli for each of the seven XLRs subjects. The red and blue boxes indicate the range of thresholds for the control group (minimum to maximum) and the horizontal lines mark the mean control thresholds. For both stimulus wavelengths, the XLRs subjects' thresholds ranged from normal to slightly elevated. Specifically, two of the XLRs subjects had slight threshold elevations (outside of the normal range) for the long-wavelength stimulus, and four XLRs subjects had slight elevations for the short-wavelength stimulus. In addition, the threshold difference between the long- and short-wavelength stimuli was approximately 2.6 log units for both subject groups. This finding is expected and indicates that thresholds for both stimuli are rod-pathway mediated. Specifically, for these stimuli that are photopically matched in luminance, the rods are expected to be over 2 log units more sensitive to the short-wavelength stimulus compared to the long-wavelength stimulus (based on the V_{λ}). A two-way repeated measures ANOVA was performed to compare thresholds for the two subject groups obtained with the two wavelengths. Specifically, subject group (XLRs vs. control) and stimulus wavelength (short vs. long) were included as main effects. The ANOVA indicated no significant effect of subject group ($F = 3.57$, $P = 0.08$) and a significant effect of wavelength ($F = 4995.80$, $P < 0.001$); the interaction between subject group and wavelength was not significant ($F = 0.66$, $P = 0.43$). Thus, these data indicate that full-field, dark-adapted luminance thresholds are normal, or nearly normal, in XLRs subjects.

Comparisons Among Measures

Figure 6 illustrates the relationships between the PLR and ERG data (left column), between the PLR and the FST

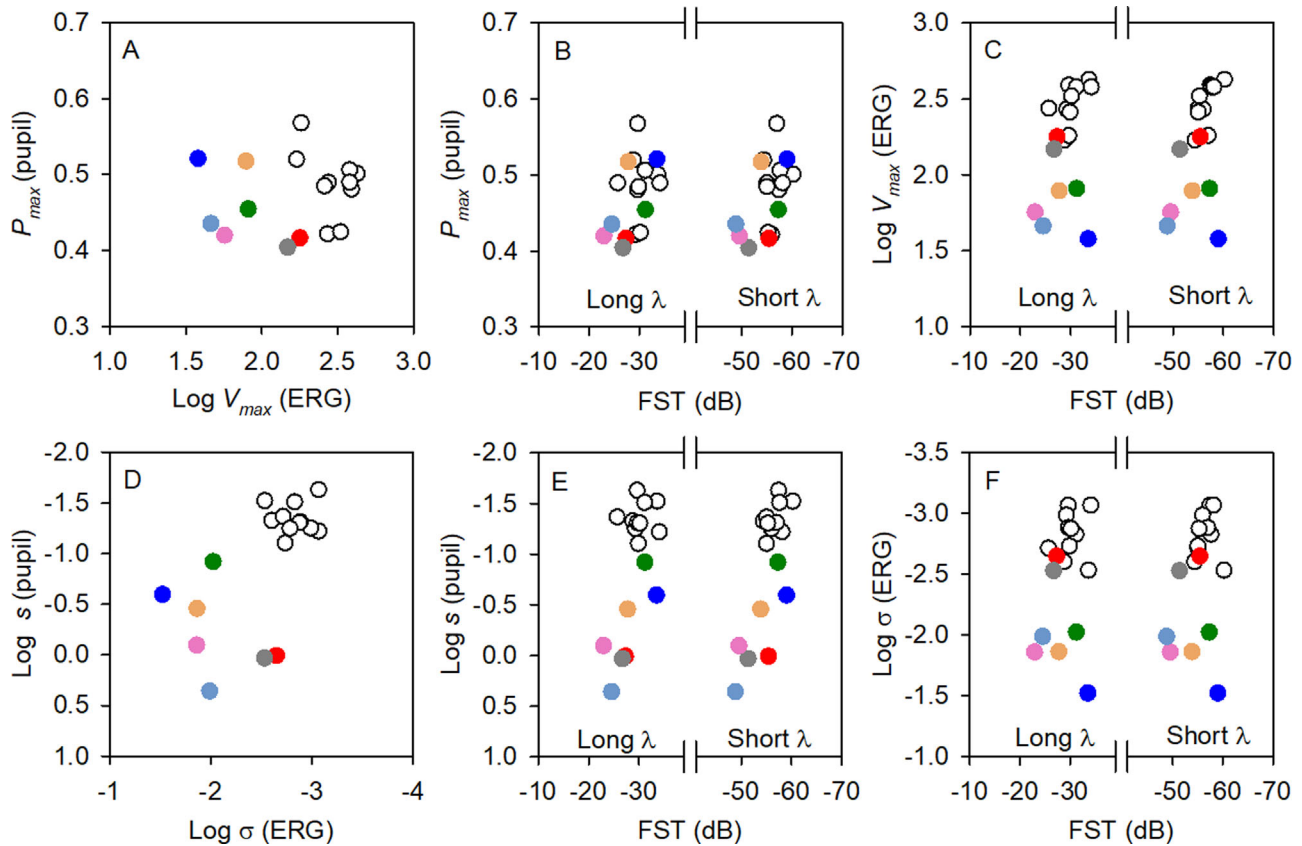


FIGURE 6. Correlations among measures. Maximum pupil response is plotted as a function of the maximum ERG b-wave amplitude (**A**) and FST threshold (**B**). In **B**, the left dataset represents the FST threshold measured with the long-wavelength stimulus, and the right dataset represents the FST threshold measured with the short-wavelength stimulus. (**C**) Maximum b-wave amplitude as a function of the long-wavelength (*left*) and short-wavelength (*right*) FST threshold. Pupil sensitivity is plotted as a function of the ERG b-wave sensitivity (**D**) and FST threshold (**E**). In **E**, the left dataset represents the FST threshold measured with the long-wavelength stimulus, and the right dataset represents the FST threshold measured with the short-wavelength stimulus. (**F**) The b-wave sensitivity as a function of the long-wavelength (*left*) and short-wavelength (*right*) FST thresholds.

data (middle column), and between the ERG and FST data (right column). **Figure 6A** shows that there is no significant correlation between the maximum PLR amplitude (P_{\max}) and maximum b-wave amplitude ($\log V_{\max}$) for the XLRs subjects ($r = -0.54$, $P = 0.21$). Of note, the differences in P_{\max} among the XLRs subjects were small (approximately 12%), whereas V_{\max} differed considerably among the XLRs subjects (approximately 1.1 log units). **Figure 6B** shows the relationship between P_{\max} and FST threshold measured with both the long-wavelength stimulus (left dataset; $r = -0.64$, $P = 0.12$) and short-wavelength stimulus (right dataset; $r = -0.58$, $P = 0.17$). Despite the moderate r values, the correlations did not achieve statistical significance. **Figure 6C** shows no significant correlation between $\log V_{\max}$ and FST measured with either the long-wavelength stimulus (left dataset; $r = 0.15$, $P = 0.76$) or the short-wavelength stimulus (right dataset; $r = -0.01$, $P = 0.98$).

Figure 6D shows that there is no significant correlation between PLR $\log s$ and b-wave $\log \sigma$ ($r = -0.44$, $P = 0.32$). In contrast, **Figure 6E** shows that pupil $\log s$ and FST threshold were correlated significantly for the XLRs subjects for both the long-wavelength stimulus (left dataset; $r = 0.77$, $P = 0.04$) and short-wavelength stimulus (right dataset; $r = 0.79$, $P = 0.03$). **Figure 6F** shows no significant correlation between ERG $\log \sigma$ and FST threshold measured with either

the long-wavelength stimulus (left dataset; $r = -0.32$, $P = 0.48$) or short-wavelength stimulus (right dataset; $r = -0.21$, $P = 0.66$). Taken together, the data indicate that only pupil sensitivity is correlated with FST threshold (**Fig. 6E**); no other correlation was statistically significant for the XLRs subjects.

DISCUSSION

This study evaluated three full-field, dark-adapted functional measures in XLRs subjects: ERG, PLR, and luminance threshold. ERG data obtained under conditions similar to those used here have been reported recently in young XLRs subjects,¹⁷ and our data confirm and extend these previous ERG findings to an adult sample of subjects. Specifically, both the present dataset and previous work show that the b-wave abnormalities in XLRs are best characterized by both reduced maximum saturated responses and sensitivity loss. To our knowledge, we show for the first time that the response of the pupil to full-field flashes of light can also be abnormal in XLRs subjects. The abnormality is most apparent for low to moderate luminance flashes, with less (or no) abnormality for high-luminance flashes. In addition, we show that the dark-adapted luminance threshold is generally normal, or nearly so, for full-field short- and long-wavelength stimuli. This finding is consistent with previ-

ous work that used spatially discrete targets (Goldmann size V) presented along the horizontal and vertical visual field meridians under dark-adapted conditions.⁷

The three functional measures used in the present study provide insight into different aspects of abnormality within the visual pathways of XLRS subjects. That is, the ERG b-wave analysis suggests an ON bipolar-cell abnormality. In addition, the photopic a-wave, b-wave, and flicker responses were also abnormal in some, but not all, subjects. Abnormalities that arise within the ON bipolar-cell response are expected based on previous work that has localized protein deficiency and structural abnormality to the photoreceptor-rod bipolar cell synapse.⁸ Indeed, a common clinical feature in XLRS subjects is an “electronegative” response in which the dark-adapted b-wave amplitude is reduced more than the a-wave amplitude (this response pattern is apparent in Fig. 1B). Thus, our subjects showed the typical ON bipolar-cell dysfunction as assessed by ERG that is associated with XLRS.

The pathway that generates the PLR is more complex than that of the ERG, and this response can provide insight into both photoreceptor/bipolar and later (ganglion cell and subcortical) stages of the visual pathway. Like the ERG, the response of the pupil to flashes of light was abnormal in our sample of XLRS subjects; however, the abnormality was most apparent at low to moderate flash luminance levels. High-luminance flashes appear to largely overcome the abnormality, and each XLRS subject had a P_{\max} that was normal or within 2% of the lower limit of normal. If higher luminance flashes had been used, P_{\max} may have fallen into the normal range for the three XLRS subjects who had slightly reduced P_{\max} . This is a somewhat surprising result, as no flash strength would generate a normal ERG b-wave amplitude in these subjects. It is possible that differences in spatial/temporal summation or gain characteristics within the PLR versus ERG generators could account for the normal PLR and abnormal b-wave for high-luminance stimuli; for example, there may be greater amplification at later stages of the visual pathway (e.g., retinal ganglion cells) that overcome the abnormality imposed at the photoreceptor/bipolar cell level. However, this is speculative, and further investigation is needed to better understand the differences between the pattern of PLR and ERG abnormality.

The pupil response elicited by the short-wavelength 450-cd/m² flash (i.e., the melanopsin condition) was generally normal for the XLRS subjects, consistent with their long-wavelength 450-cd/m² responses. This suggests that inner-retina function, inferred by ipRGC function, is largely normal in these individuals. The exception was XLRS6, who had a slightly reduced PIPR, which may indicate ipRGC dysfunction in this individual. It would be of interest to evaluate the extent of inner-retina dysfunction in our sample of XLRS subjects using the pattern ERG (pERG), which is also a measure of RGC function. In a large sample of individuals with XLRS (N = 44), the pERG was found to be abnormal in nearly all subjects.³⁰ Although this finding appears to conflict with our generally normal PIPR results, there are several important differences between the pERG and PIPR. For example, the PIPR is generated by a small subset of RGCs (ipRGCs) in response to a high-luminance, full-field flash, whereas the pERG is generated by conventional RGCs (non-ipRGCs) in response to contrast-reversing spatial stimuli presented within the macula. Furthermore, the pERG is highly sensitive to disturbances at preceding retinal sites (e.g., cone photoreceptors, bipolar cells), whereas the PIPR

may have somewhat less dependency. Thus, the pERG and PIPR may provide insight into different aspects of inner-retina function, which could be of value in future studies of XLRS.

Each of the measures reported in the present study was elicited by full-field stimuli. Full-field stimuli may be of practical use in assessing visual function in XLRS subjects and in other patient populations. For example, one advantage of full-field stimulation is that steady foveal fixation is not essential, which could be important in subjects who have large cystic-appearing lesions at the fovea and use a non-foveal fixation location. Likewise, careful optical refraction is not essential, as the ERG, PLR, and FST are unlikely to be affected markedly by refractive error. A fundamental limitation of Ganzfeld stimulation, however, is the inability to map abnormalities throughout the visual field. In fact, a small region of the visual field that functions normally may generate a normal FST threshold; the use of a full-field stimulus precludes determining how much of the visual field is normal or abnormal. Thus, the selection of the most appropriate measure can be guided by (1) the importance of a spatially localized versus full-field response; and (2) the need to determine the stage at which function is affected (e.g., retina only, given by the ERG; retina and extra-retina non-image-forming sites, given by the PLR; complete visual pathway, given by the FST).

In summary, the ERG and PLR can be abnormal in XLRS subjects, but the extent of these abnormalities is not strongly correlated. By contrast, the dark-adapted luminance threshold is generally normal, or only modestly elevated, in these individuals. Luminance threshold is correlated with pupil response sensitivity. The results indicate that the ERG, PLR, and FST provide different views of abnormality in XLRS and that these measures may be of use in future clinical trials.

Acknowledgments

The authors thank Neal Peachey, PhD, for comments on the manuscript and Nicole Sabbia for assistance with subject recruitment.

Supported by grants from the National Institutes of Health (R01EY029796 and P30EY001792); The Pangere Family Foundation; unrestricted funds from Research to Prevent Blindness to the Department of Ophthalmology and Visual Sciences, University of Illinois at Chicago.

Disclosure: **J.J. McAnany**, None; **J.C. Park**, None; **G.A. Fishman**, None; **F.T. Collison**, None

References

1. Sauer CG, Gehrig A, Warneke-Wittstock R, et al. Positional cloning of the gene associated with X-linked juvenile retinoschisis. *Nat Genet.* 1997;17:164–170.
2. Sieving PA, MacDonald IM, Chan S. X-linked juvenile retinoschisis. In: Adam MP, Ardinger HH, Pagon RA, et al., eds. *GeneReviews*[®]. Seattle, WA: University of Washington, Seattle; 1993.
3. Wang T, Zhou A, Waters CT, O'Connor E, Read RJ, Trump D. Molecular pathology of X linked retinoschisis: mutations interfere with retinoschisin secretion and oligomerisation. *Br J Ophthalmol.* 2006;90:81–86.
4. George ND, Yates JR, Moore AT. X linked retinoschisis. *Br J Ophthalmol.* 1995;79:697–702.

5. Roesch MT, Ewing CC, Gibson AE, Weber BH. The natural history of X-linked retinoschisis. *Can J Ophthalmol*. 1998;33:149–158.
6. Bowles K, Cukras C, Turriff A, et al. X-linked retinoschisis: RS1 mutation severity and age affect the ERG phenotype in a cohort of 68 affected male subjects. *Invest Ophthalmol Vis Sci*. 2011;52:9250–9256.
7. Peachey NS, Fishman GA, Derlacki DJ, Brigell MG. Psychophysical and electroretinographic findings in X-linked juvenile retinoschisis. *Arch Ophthalmol*. 1987;105:513–516.
8. Ou J, Vijayasathy C, Ziccardi L, et al. Synaptic pathology and therapeutic repair in adult retinoschisis mouse by AAV-RS1 transfer. *J Clin Invest*. 2015;125:2891–2903.
9. Liu Y, Kinoshita J, Ivanova E, et al. Mouse models of X-linked juvenile retinoschisis have an early onset phenotype, the severity of which varies with genotype. *Hum Mol Genet*. 2019;28:3072–3090.
10. Khan NW, Jamison JA, Kemp JA, Sieving PA. Analysis of photoreceptor function and inner retinal activity in juvenile X-linked retinoschisis. *Vision Res*. 2001;41:3931–3942.
11. Bennett LD, Wang YZ, Klein M, Pennesi ME, Jayasundera T, Birch DG. Structure/psychophysical relationships in X-linked retinoschisis. *Invest Ophthalmol Vis Sci*. 2016;57:332–337.
12. Collison FT, Park JC, Fishman GA, Stone EM, McAnany JJ. Two-color pupillometry in KCNV2 retinopathy. *Doc Ophthalmol*. 2019;139:11–20.
13. Collison FT, Park JC, Fishman GA, Stone EM, McAnany JJ. Two-color pupillometry in enhanced S-cone syndrome caused by NR2E3 mutations. *Doc Ophthalmol*. 2016;132:157–166.
14. Collison FT, Park JC, Fishman GA, McAnany JJ, Stone EM. Full-field pupillary light responses, luminance thresholds, and light discomfort thresholds in CEP290 Leber congenital amaurosis patients. *Invest Ophthalmol Vis Sci*. 2015;56:7130–7136.
15. Gamlin PD, McDougal DH, Pokorny J, Smith VC, Yau KW, Dacey DM. Human and macaque pupil responses driven by melanopsin-containing retinal ganglion cells. *Vision Res*. 2007;47:946–954.
16. Kardon R, Anderson SC, Damarjian TG, Grace EM, Stone E, Kawasaki A. Chromatic pupil responses: preferential activation of the melanopsin-mediated versus outer photoreceptor-mediated pupil light reflex. *Ophthalmology*. 2009;116:1564–1573.
17. Ambrosio L, Hansen RM, Kimia R, Fulton AB. Retinal function in X-linked juvenile retinoschisis. *Invest Ophthalmol Vis Sci*. 2019;60:4872–4881.
18. Johnson MA, Jeffrey BG, Messias AMV, Robson AG. ISCEV extended protocol for the stimulus-response series for the dark-adapted full-field ERG b-wave. *Doc Ophthalmol*. 2019;138:217–227.
19. Peachey NS, Alexander KR, Fishman GA. The luminance-response function of the dark-adapted human electroretinogram. *Vision Res*. 1989;29:263–270.
20. Dacey DM, Liao HW, Peterson BB, et al. Melanopsin-expressing ganglion cells in primate retina signal colour and irradiance and project to the LGN. *Nature*. 2005;433:749–754.
21. Park JC, Moura AL, Raza AS, Rhee DW, Kardon RH, Hood DC. Toward a clinical protocol for assessing rod, cone, and melanopsin contributions to the human pupil response. *Invest Ophthalmol Vis Sci*. 2011;52:6624–6635.
22. Kelbsch C, Strasser T, Chen Y, et al. Standards in pupillography. *Front Neurol*. 2019;10:129.
23. Park JC, Chen YF, Blair NP, et al. Pupillary responses in non-proliferative diabetic retinopathy. *Sci Rep*. 2017;7:44987.
24. Park JC, McAnany JJ. Effect of stimulus size and luminance on the rod-, cone-, and melanopsin-mediated pupillary light reflex. *J Vis*. 2015;15:13.
25. Roman AJ, Cideciyan AV, Aleman TS, Jacobson SG. Full-field stimulus testing (FST) to quantify visual perception in severely blind candidates for treatment trials. *Physiol Meas*. 2007;28:N51–N56.
26. McCulloch DL, Marmor MF, Brigell MG, et al. ISCEV standard for full-field clinical electroretinography (2015 update). *Doc Ophthalmol*. 2015;130:1–12.
27. Eksandh L, Andreasson S, Abrahamson M. Juvenile X-linked retinoschisis with normal scotopic b-wave in the electroretinogram at an early stage of the disease. *Ophthalmic Genet*. 2005;26:111–117.
28. Eksandh LC, Ponjavic V, Ayyagari R, et al. Phenotypic expression of juvenile X-linked retinoschisis in Swedish families with different mutations in the XLR51 gene. *Arch Ophthalmol*. 2000;118:1098–1104.
29. Molday RS, Kellner U, Weber BH. X-linked juvenile retinoschisis: clinical diagnosis, genetic analysis, and molecular mechanisms. *Prog Retin Eye Res*. 2012;31:195–212.
30. Vincent A, Robson AG, Neveu MM, et al. A phenotype-genotype correlation study of X-linked retinoschisis. *Ophthalmology*. 2013;120:1454–1464.